Int. J. Electrochem. Sci., 12 **(2017)** 5731 – 5741, doi: 10.20964/2017.06.41

International Journal of
ELECTROCHEMICAL
SCIENCE
www.electrochemsci.org

Effects of Carbon Hosts on Electrochemical Properties of Lithium-Sulfur Batteries

Tao Li[1,2], *Hong Bo*[1,4,*], *Huawei Cao*[2], *Yanqing Lai* [1], *Yexiang Liu*[1], *Zixin Huang*[3]

[1] School of Metallurgy and Environment, Central South University, Changsha, Hunan 410083, China
[2] Shenzhen Perfect Power Technology Co., Ltd, Shenzhen, 518057, China
[3]Engineering Research Center of High Performance Battery Materials and Devices, Research Institute of Central South University in Shenzhen, Shenzhen, 518057, China
[4] School of Materials Science and Engineering, Central South University, Changsha, Hunan 410083, China
[*]E-mail: bop_hong@163.com

Received: 8 January 2017 / *Accepted:* 9 April 2017 / *Published:* 12 May 2017

Three kinds of sulfur cathodes based on different carbon hosts were prepared for lithium-sulfur battery. Effects of carbon hosts on composite structure and cell performance were attentively investigated. The hierarchically porous Ketjen black (ECP) owns higher specific surface area and pore volumes than Super P (SP), thus increasing active material utilization, but incapable of restraining rapid capacity fading. When carbon nanotube (CNT) was used for loading sulfur, sulfur can penetrate adequately into CNT and merge with it completely, which forms strong interaction between them. It helps to trap sulfur or reaction intermediates, and accommodates volume changes of sulfur upon cycling. Besides, the highly conductive CNT favors less polarization and better redox reversibility. These factors together promote electrochemical performance of the cathode. A high reversible capacity of 725 mAh g^{-1} and capacity retention of ~80% (based on 2nd discharge) is obtained after 100 cycles for the CNT-S composite. The work guides us how to treat rationally the porous structure when considering suitable carbon material for lithium sulfur batteries.

Keywords: carbon nanotube; porous structure; specific surface area; lithium sulfur battery; electrochemical performance

1. INTRODUCTION

As a light-weight element, sulfur can react with metallic lithium to form lithium sulfide by two-electron reaction, generating a high theoretical capacity of 1675 mAh g^{-1} and high theoretical energy density of 2500 Wh kg^{-1} in a lithium-sulfur (Li-S) battery [1]. Therefore, intensive efforts have been

devoted to developing this promising battery system, in order to meet the burgeoning need of electric vehicles. However, the incredible performance of the battery is hindered by several defects, such as the insulating nature of sulfur, dissolution of intermediates, shuttle effect between two electrodes, and irreversible deposition of reaction byproducts [2-4].

Various carbon materials have been proved to be effective and facile candidates to tackle the above problems, including carbon black, mesoporous carbon, carbon nanofiber, carbon nanotube, and graphene nanosheet [5-8]. The benefits of combining sulfur with carbon matrix is not only improving the electronic conductivity but also reduces the loss of active material by encapsulating soluble polysulfides within the carbon framework [9]. Designing a carbon material with required morphology, reasonable porosity and high conductivity are of great significance to achieve excellent electrochemical performance. However, the detailed comparison on the physical and electrochemical properties of sulfur-carbon composites constructed by various conductive carbons was short of reports at present.

In this work, three common carbon materials--carbon nanotube (CNT), Ketjen black (ECP) and Super P (SP) were chose as host for sulfur, respectively. The effect of carbon type on composite structure and cell performance were investigated. The research reminds us that the structure parameters, such as pore size distribution (PSD), pore volume (V_T) and specific surface area (SSA), need to be considered when selecting proper carbon host for Li-S batteries, but are not exclusive in determining cell properties. Other some factors (e.g., electronic conductivity, interaction between sulfur and carbon, the location of sulfur within carbon) influence greatly the electrochemical performances of Li-S batteries as well.

2. EXPERIMENTAL

2.1. Synthesis of sulfur/carbon composite

The CNT-S composite was prepared by a simple melting-infusion strategy. 25 wt% of carbon nanotube and 75wt% of sulfur were mixed in an agate mortar homogeneously, then the obtained powder was put in a stainless-steel container, preserved at 155 ºC for 12 hours, followed by another 2 hours at 250 ºC.

For comparison, CNT was replaced by ECP and SP respectively, and other synthesis procedure is similar to the above. The resultant composite was marked as ECP-S and SP-S, respectively.

2.2. Electrode fabrication and cell assembly

The obtained sulfur/carbon composite was mixed with SP and poly(vinylidene fluoride) (PVDF) in a weight ratio of 8: 1: 1 in N–methylpyrrolidone (NMP) to form homogeneous slurry. Then the slurry was spread onto a carbon-coated aluminum foil by a doctor blade and dried at 60 ºC overnight. The electrode was cut into pellets with a diameter of ~1.4 cm and the sulfur loading on each disk is typically 1~1.5 mg cm^{-2}.

CR2025 coin cells were assembled in an Ar-filled glove box, with lithium metal as counter electrode and reference electrode and Celgard 2400 as separator. The electrolyte consisted of 1M lithium bis(trifluoromethane sulfonel)imide (LiTFSI) in a mixed solvent of 1,2-dimethoxyethane (DME) and 1,3-dioxolane (DOL) at a volume ratio of 1:1, including 0.1 M lithium nitrate ($LiNO_3$) as additive. The ratio of electrolyte volume to sulfur loading on the cathode was controlled to be ~12 uL mg^{-1}.

2.3. Characterization and electrochemical measurement

Thermo gravimetric analysis (TGA) was conducted in investigating sulfur content in the composites at 10 ºC min^{-1} heating rate under flowing N_2. Powder X-ray diffraction (XRD) patterns of various carbons and composites were collected with CuKa radiation. The morphologies of various carbons and composites was observed on scanning electron microscopy (SEM) and high-resolution transmission electron microscopy (HRTEM), combined with energy dispersive X-ray spectroscopy (EDX) for element distribution detection. Nitrogen adsorption/desorption isotherms were obtained by Quanta chrome instrument at 77 K. Electrical resistivity of the cathode was achieved by a four-probe method. Each data presented in the paper is an average value based on three tests.

Galvanostatic charge/discharge tests were carried out to check the reversible capacity and cycle stability of the cathodes at ambient temperature using LAND instrument in the potential range of 1.7~2.8 V. Cyclic voltammetry (CV) measurement was conducted on a Solartron 1470E electrochemical workstation at a scan rate of 0.1 mV s^{-1}. Electrochemical impedance spectroscopy (EIS) was measured over a frequency range of 10^5 Hz to 0.01 Hz at an amplitude of 5 mV.

3. RESULTS AND DISCUSSION

TGA results of three S-C composites are shown in Fig.1a. The curve depicts weight losses of the composite correlated to the evaporation of sulfur under N_2 atmosphere, while the carbon is responsible for all of the residual weight. Thus the sulfur content in these composites all reaches around 75%, close to the original design of fabricating these composites. XRD patterns of sublimed sulfur, various carbons and composites are shown in Fig. 6b, 6c and 6d. For elemental sulfur, the sharp and strong peaks at 23°~29° reflect a very stable Fddd orthorhombic crystalline structure [10]. Three carbons all exhibit amorphous but partially graphitized structure with two broad peaks at around 25° and 44°, responsible for (002) and (100) diffraction respectively [11]. After loading sulfur, the patterns of these composites present plenty of characteristic peaks similar to sulfur (except for low intensity). It is suggested that no phase transformation occurs during heat treatment and some sulfur crystals would be deposited on the carbon surface, agreement with the reports on high sulfur loading [12].

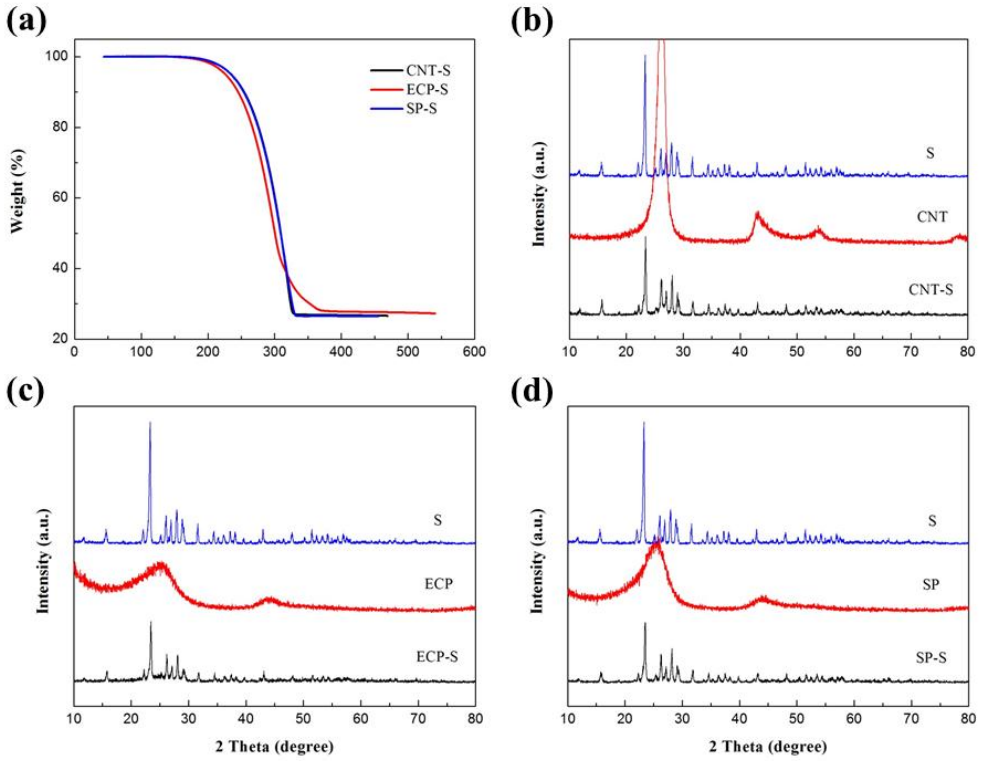

Figure 1. (a) TGA curves of different composites; XRD patterns for (b) CNT, CNT-S, (c) ECP, ECP-S and (d) SP, SP-S

Nitrogen adsorption–desorption measurements were employed to investigate the textural properties of various carbons and resultant composites. As shown in Fig.2a, 2b and 2c, the isotherms of three carbons can be identified as type IV according to IUPAC classication, indicating well-developed mesoporous networks [13]. The obvious hysteresis loop displayed in the desorption branch of ECP suggests that it possesses larger volume of mesopores compared with other two carbons [14]. The PSD plots based on density functional theory calculation are shown in Fig.2d, 2e and 2f. The SSA and V_T values of various carbon and composites and summarized in Table S1. ECP owns lager SSA and V_T than other carbons, which can provide sufficient rooms for sulfur loading and act as pathways for electrolyte diffusion. The wide distribution in pore size from 2nm to 250nm indicates that ECP is hierarchically porous, contributed by the interspaces between ECP nanoparticles. For CNT, there were large amount of meso- and macropores in the range below 100nm. For SP, its SSA is significantly lower than ECP, accompanied by a relatively narrow PSD. It is noted that after loading sulfur into carbon, the SSA and V_T of as-prepared three composites all decreases dramatically, suggesting that most of pores in these carbons are occupied by elemental sulfur during heat treatment. Considering the residual SSA and V_T values, ECP and CNT may still remain some unfilled yields, which allows electrolyte to infiltrate and helps to maintain a good mass transport within the structure. Yet the pore volume of SP nearly accommodates sulfur fully because of the absence of residual pores in the composite.

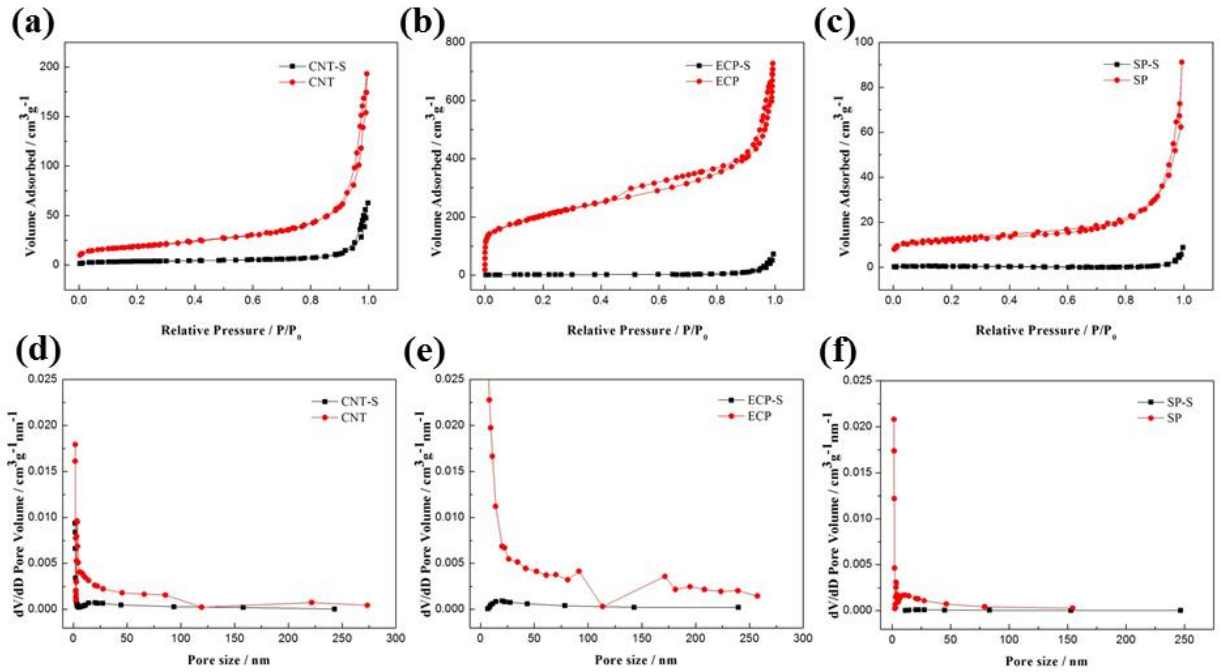

Figure 2. N_2 adsorption–desorption isotherm plots of (a) CNT, CNT-S, (b) ECP, ECP-S and (c) SP, SP-S; Pore size distributions of (d) CNT, CNT-S, (e) ECP, ECP-S and (f) SP, SP-S

Various carbon hosts and as-prepared composites were observed by SEM and the results are presented in Fig.3. The CNTs (Fig.3a) with good one-dimensional nanostructure create a complicated network with abundant pores. The ECP (Fig.3b) and SP (Fig.3c) are sphere-like, presenting porous characteristics due to the interspaces between nanoparticles. The sulfur loading seems to have little effect on the overall morphology of CNT (Fig.3d). For ECP (Fig.3e), High SSA provides favorable environment for sulfur, hence most of elemental sulfur is filled within the various pores. Certain agglomerates exist in the SP-S composite (Fig.3f), because SP only possesses limited inner spaces for sulfur, producing exterior growth. These are well consistent with PSD results above.

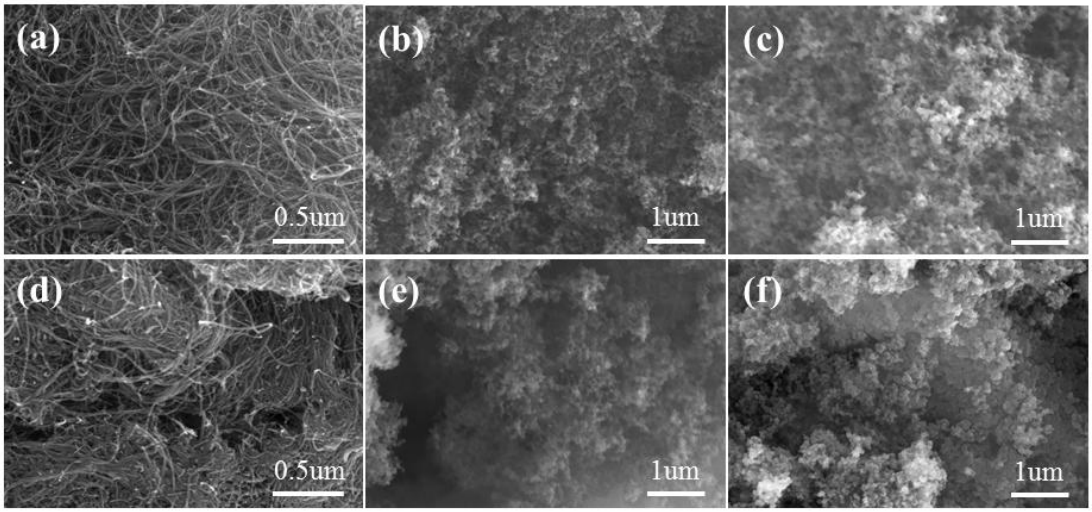

Figure 3. SEM images of (a) CNT, (b) ECP, (c) SP, (d) CNT-S, (e) ECP-S and (f) SP-S

The microstructures of various composites were further characterized by HRTEM. CNT has a typical pipe structure with a diameter of ~60 nm (Fig.S1). No bulk sulfur particle is found among the CNTs from Fig.4a, so there is no distinct morphological difference between CNT and CNT-S composite. Further magnified image (Fig.4d) indicates that the CNT-S has defective walls as well as localized graphitic areas [15], and its mesoporous structure is confirmed. Certain amount of sulfur is coated uniformly on the surface of tube wall, forming a thin layer with several nm's thickness. As elemental sulfur has a nature of low surface tension on carbon. When sulfur is in molten state, CNT serves as the support. Sulfur deposits on its surface, and then grows up to wrap the whole wall [16]. In addition, plenty of sulfur particles seem to permeate into the internal of CNT, because some lattice fringes [17, 18] are distinguishable in the area, while sulfur is highly crystallized (as supported by previous XRD test). More convictive evidence of sulfur's existence in the CNT-S composite is provided by the EDX mapping. A single CNT-S composite was selected for this analysis. Fig.4g demonstrates that sulfur is well distributed throughout the whole nanotube, including inside and outside the wall. Thus it is strongly conformed that a part of sulfur is effectively confined within the tube. It should be noted that rapid ion transport to the sulfur inside the wall is still feasible because Li ion is capable of easily penetrating the thin carbon wall.

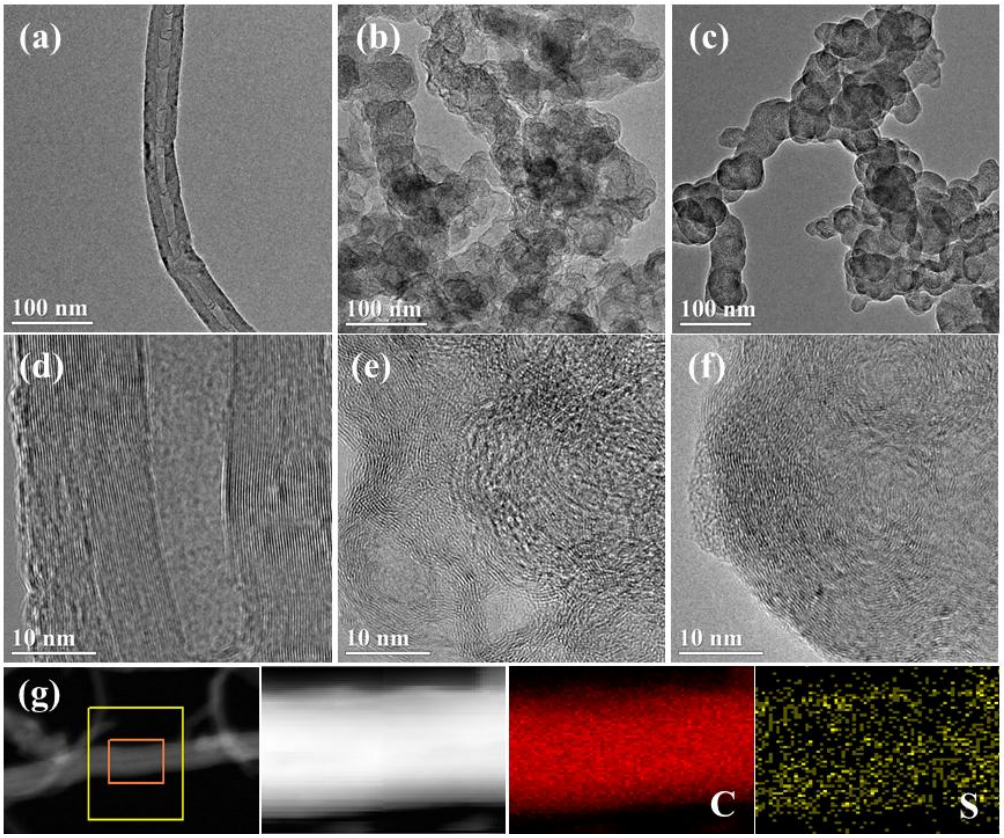

Figure 4. HRTEM images of (a, d) CNT-S, (b, e) ECP-S and (c, f) SP-S; (g) EDX mapping of single CNT-S composite

By contrast, ECP-S (Fig.4b) and SP-S (Fig.4c) actually compose of very fine bead-like chains [16]. More careful observation finds well-resolved lattice fringes of crystalline sulfur and amorphous carbon (Fig.4e and 4f). Obviously, sulfur particles are coated on the carbon surface. The reason is similar to that of CNT-S. The attached sulfur to the exterior surface of the porous carbon results in conglutination of the composite particles and lowers SSA of the material [18]. Hence the aggregation of nano-sized spherical particles is visible (especially for SP-S). The core-shell structure with dense sulfur shells enclosing carbon cores achieves contact between conductive carbon and sulfur, providing electron pathways for the insulated sulfur.

CV profiles of different composite cathodes are shown in Fig.5a. Two main reduction peaks at around 2.3 and 2.0 V were detected during the first cathodic scan, corresponding to conversion of elemental sulfur to polysulfides and then to sulfides, respectively [19]. For CNT-S, two oxidation peaks at 2.35 and 2.42 V in the subsequent anodic scan were identified, standing for the transition of lithium sulfide to polysulfides and further to the final oxidized active sulfur, respectively [20]. But ECP-S and SP-S only generate an oxidation peak, which can be understood as the overlapping of above two peaks [21]. The two reduction peaks linked to CNT-S locate in the higher potential sites and its oxidation peaks located lower compared to other two cases, reflecting better redox reversibility. This conclusion is further supported by potential curves of these composite cathodes. As shown in Fig.5b, the comparison of discharge-charge plateaus among the three cathodes is well consistent with that of the oxidation-reduction peaks from CV tests. This is because CNT possess excellent conductivity among the three carbons, meanwhile the complete and compact contact between sulfur and CNT are established in the composite, facilitating the electronic transport. A simple resistivity test initiated by four-probe method demonstrates that the CNT-S cathode has an electrical resistivity of 5.97 Ω·cm, lower than that of ECP-S and SP-S cathode (6.77 and 7.85, respectively). Thus less polarization and better electrochemical properties appears in CNT-S cathode.

Fig. 5c presents the cycle performance of different cathodes during cycling at a rate of 0.2 C. The initial capacity is quite low and preserved capacity is only 580 mAh g^{-1} after 50 cycles for SP-S, reflecting limited promotion ability to electrochemical activity of sulfur by SP. For comparison, the active material utilization in the cathode is greatly improved if using ECP as conductive host. It is benefited from the well-distribution of sulfur particles inside hierarchical pores of ECP, enhancing ion transport and charge transfer in the cathode. But rapid capacity fading still exists to some extent for the composite cathode, which illustrates that high SSA and pore-rich structure of carbon material is not exclusive for the cycle stability of the composite cathode. For CNT-S, a high initial capacity of 1054 mAh g^{-1} and reversible capacity of up to 725 mAh g^{-1} after 100 cycles are obtained. The inevitable dissolution of polysulfides into the electrolyte [22] causes a part of capacity loss during the first two cycles, but the satisfactory cycle capability can be obtained at subsequent cycles (the capacity retention reaches almost 80% based on 2nd discharge capacity). Furthermore, the stable charge-discharge plateaus can be maintained over the whole cycle period (as shown in Fig.5d). The excellent cycle stability of CNT-S should be attributed to two aspects below. On the one hand, the adequate penetration sulfur into CNT and merging between them helps to trap sulfur and reaction intermediates and suppress undesired side reactions associated with polysulfides by physical or chemical absorption.

On the other hand, the mechanical stress induced by volume changes of sulfur during cycling can be accommodated by the particular structure [23].

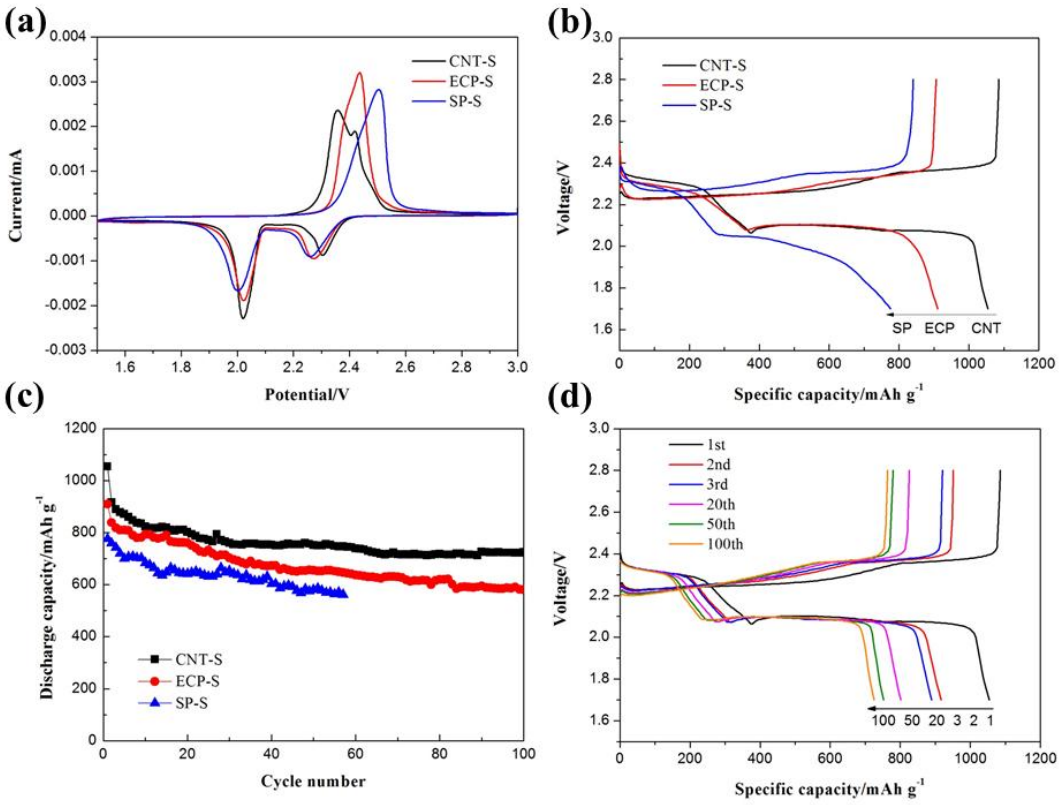

Figure 5. (a) CV profiles, (b) potential curves and (c) cycle performances of different cathodes during cycling; (d) charge-discharge curves of CNT-S cathode

EIS was measured on the cathode before and after cycles in order to further understand the effect of carbon type on the cell performance. As shown in Fig.6a, the impedance spectrum of CNT-S cathode owns a smaller high-frequency semicircle than that of other two cathodes. Since the semicircle in the high frequency region is related to the interface charge-transfer resistance (R_{ct}) [24], the decreased width of semicircle exhibited by the CNT-S indicates better conduction between particles, likely originating from the uniform distribution of sulfur in the composite and strong interaction between sulfur and CNT. In addition, the porous network constructed by the nanotubes and the thin tube wall also provide convenient ion transport pathway. The drastic decline of R_{ct} after cycles is probably attributed to the redistribution of sulfur in the carbon matrix and the penetration of the electrolyte into the electrode [25]. An additional semicircle appears in the high-middle frequency region after cycles (Fig.6b), which is always associated with Li^+ migration through the solid-electrolyte interface (SEI) layer formed on the electrode (R_s) [26]. It is assumed that the CNT-S and ECP-S composite still have certain amount of pore spaces for the deposition of insoluble sulfides, hence contribute to relatively thinner SEI and smaller R_s than SP-S. It favors the stability of electrode structure and in turn improves the electrochemical performance of the cell.

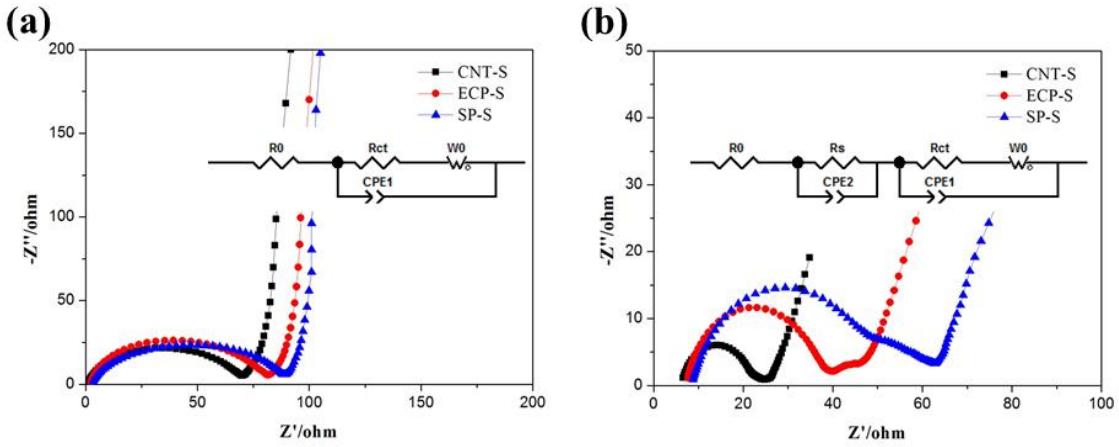

Figure 6. Nyquist plots of different composite cathodes (a) before cycle and (b) after cycles

4. CONCLUSIONS

Significant effects of carbon type on the structure and properties of S-C composite have been demonstrated in this study. ECP is hierarchically porous with wide PSD and high SSA, which provides sufficient rooms for sulfur loading and ion diffusion. While the pore structure of SP is relatively weak, thus agglomerates exist in the SP-S composite. As for CNT-S, certain amount of sulfur is coated uniformly on the surface of tube wall, and others permeate into the internal of CNT. Thus sulfur is well distributed throughout the whole carbon tube and compact contact between them is achieved. The CNT-S cathode exhibits best electrochemical performance among three cases, even though the structure parameters of CNT seem to be lack of advantages compared to ECP.

SUPPORT INFORMATION

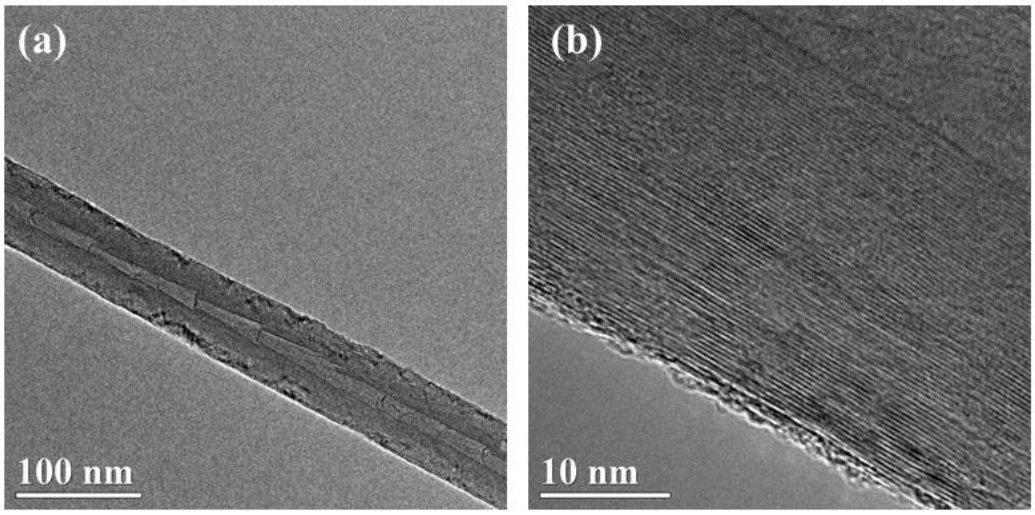

Fig.S1 HRTEM images of CNT-S: (a) low magnification; (b) high magnification

Table S1 Key pore parameters of various carbons and composites

Materials	SSA (m^2 g^{-1})	V_T (ml g^{-1})
CNT-S	12.85	0.0970
ECP-S	6.67	0.1127
SP-S	1.78	0.0137
CNT	65.50	0.2987
ECP	632.67	1.1248
SP	43.77	0.1410

ACKNOWLEDGMENTS
The authors thank the financial support of National Natural Science Foundation of China (51474243 and 51574288) and Strategic Emerging Industries Program of Shenzhen (JCYJ20120618164543322).

References

1. L. Ma, K.E. Hendrickson, S. Wei and L.A. Archer, *Nano Today*, 10 (2015) 315.
2. A. Manthiram, Y. Fu, S.H. Chung, C. Zu and Y.S. Su, *Chem. Rev.*, 114 (2014) 11751.
3. Y. Diao, K. Xie, X. Hong and S. Xiong, *Acta Chim. Sinica*, 71 (2013) 508.
4. H. Noh, J. Song, J.K. Park and H.T. Kim, *J. Power Sources*, 293 (2015) 329.
5. X. Ji, K.T. Lee, L.F. Nazar, *Nat. Mater.*, 8 (2009) 500.
6. X.B. Cheng, J.Q. Huang, Q. Zhang, H.J. Peng, M.Q. Zhao and F. Wei, *Nano Energy*, 4 (2014) 65.
7. L. Zeng, F. Pan, W. Li, Y. Jiang, X. Zhong and Y. Yu, *Nanoscale*, 6 (2014) 9579.
8. M.Q. Zhao, Q. Zhang, J.Q. Huang, G.L. Tian, J.Q. Nie, H.J. Peng and F. Wei, *Nat. Commun*., 5 (2014) 3410.
9. J. Liang, Z.H. Sun, F. Li and H.M. Cheng, *Energy Storage Mater*, 2 (2016) 76.
10. Z. Zhang, Q. Li, Y. Lai, J. Li, *J. Phys. Chem*. C, 118 (2014) 13369.
11. S. Zhao, C. Li, W. Wang, H. Zhang, M. Gao, X. Xiong, A. Wang, K. Yuan, Y. Huang and F. Wang, *J. Mater. Chem*. A, 1 (2013) 3334.
12. K. Zhang, Q. Zhao, Z. Tao, J. Chen, *Nano Res*., 6 (2012) 38.
13. Z. Zhang, Q. Li, S. Jiang, K. Zhang, Y. Lai and J. Li, *Chem. Eur. J.*, 21 (2015) 1343.
14. Q. Li, Z. Zhang, Z. Guo, K. Zhang, Y. Lai and J. Li, *J. Power Sources*, 274 (2015) 338.
15. G. Zhou, D.W. Wang, F. Li, P.X. Hou, L. Yin, C. Liu, G.Q. Lu, I.R. Gentle and H.M. Cheng, *Energy Environ. Sci*., 5 (2012) 8901.
16. C. Wang, J. Chen, Y. Shi, M. Zheng, Q. Dong. *Electrochim. Acta*, 55 (2010) 7010.
17. Y. Liu, H. Zhan, Y. Zhou, *Electrochim. Acta*, 70 (2012) 241.
18. X. Cui, Z. Shan, L. Cui, J. Tian, *Electrochim. Acta*, 105 (2013) 23.
19. S.H. Chung, A. Manthiram, *ACS Sustainable Chem. Eng*., 2 (2014) 2248.
20. L. Zhu, W Zhu, X.B. Cheng, J.Q. Huang, H.J. Peng, S.H. Yang and Q. Zhang, *Carbon*, 75 (2014) 161.
21. H. Lu, K. Zhang, Y. Yuan, F. Qin, Z. Zhang, Y. Lai and Y. Liu, *Electrochim. Acta*, 161 (2015) 55.
22. H. Lu, Y. Yuan, K. Zhang, F. Qin, Y. Lai and Y. Liu, *J. Electrochem. Soc*., 162 (2015) A1460.
23. G. Zheng, Y. Yang, J.J. Cha, S.S. Hong and Y. Cui, *Nano Lett*., 11 (2011) 4462.
24. Y. Yuan, H. Lu, Z. Fang, B. Chen, *Ionics*, 22 (2016) 1509.
25. J. Li, F. Qin, L. Zhang, K. Zhang, Q. Li, Y. Lai, Z. Zhang and J. Fang, *J. Mater. Chem*. A, 2 (2014)

13916.
26. H. Lu, Y. Yuan, Z. Hou, Y. Lai, K. Zhang and Y. Liu, *RSC Adv.*, 6 (2016) 18186.